Accepted Manuscript

Construction of an alkaline phosphatase-specific two-photon probe and its imaging application in living cells and tissues

Huatang Zhang, Peng Xiao, Yin Ting Wong, Wei Shen, Mohit Chhabra, Raoul Peltier, Yin Jiang, Yonghe He, Jun He, Yi Tan, Yusheng Xie, Derek Ho, Yun-Wah Lam, Jinpeng Sun, Hongyan Sun

PII: S0142-9612(17)30432-5

DOI: 10.1016/j.biomaterials.2017.06.032

Reference: JBMT 18152

To appear in: *Biomaterials*

Received Date: 12 February 2017

Revised Date: 8 June 2017

Accepted Date: 22 June 2017

Please cite this article as: Zhang H, Xiao P, Wong YT, Shen W, Chhabra M, Peltier R, Jiang Y, He Y, He J, Tan Y, Xie Y, Ho D, Lam Y-W, Sun J, Sun H, Construction of an alkaline phosphatase-specific two-photon probe and its imaging application in living cells and tissues, *Biomaterials* (2017), doi: 10.1016/j.biomaterials.2017.06.032.

Construction of an Alkaline Phosphatase-Specific Two-photon Probe and Its Imaging Application in Living Cells and Tissues

Huatang Zhang,[a,b] Peng Xiao,[c] Yin Ting Wong,[d] Wei Shen,[b] Mohit Chhabra,[b] Raoul Peltier,[b] Yin Jiang,[a] Yonghe He,[a] Jun He,[a] Yi Tan,[b] Yusheng Xie,[b] Derek Ho,[e] Yun-Wah Lam,[b,*] Jinpeng Sun[c,*] and Hongyan Sun[b,*]

[a] School of Chemical Engineering and Light Industry, Guangdong University of Technology, Guangzhou, Guang dong 510006, P. R. China.

[b] Department of Biology and Chemistry, City University of Hong Kong, 83 Tat Chee Avenue, Kowloon, Hong Kong, P. R. China.

[c] Department of Physiology, Shandong University School of Medicine, Jinan, Shandong 250012, P. R. China

[d] Department of Biomedical Sciences, City University of Hong Kong, 83 Tat Chee Avenue, Kowloon, Hong Kong, P. R. China

[e] Department of Physics and Materials Science, City University of Hong Kong, 83 Tat Chee Avenue, Kowloon, Hong Kong, P. R. China.

Corresponding Author: yunwlam@cityu.edu.hk;
sunjinpeng@sdu.edu.cn;
hongysun@cityu.edu.hk

Abstract

Alkaline phosphatase (ALP) is a family of enzymes involved in the regulation of important biological processes such as cell differentiation and bone mineralization. Monitoring the activity of ALP in serum can help diagnose a variety of diseases including bone and liver diseases. There has been growing interest in developing new chemical tools for monitoring ALP activity in living systems. Such tools will help further delineate the roles of ALP in biological and pathological processes. Previously reported fluorescent probes has a number of disadvantages that limit their application, such as poor selectivity and short-wavelength excitation. In this work, we report a new two-photon fluorescent

probe (TP-Phos) to selectively detect ALP activity. The probe is composed of a two-photon fluorophore, a phosphate recognition moiety, and a self-cleavable adaptor. It offers a number of advantages over previously reported probes, such as fast reaction kinetics, high sensitivity and low cytotoxicity. Experimental results also showed that TP-Phos displayed improved selectivity over DIFMUP, a commonly utilized ALP probe. The selectivity is attributed to the utilization of an ortho-functionalised phenyl phosphate group, which increases the steric hindrance of the probe and the active site of phosphatases. Moreover, the two-photon nature of the probe confers enhanced imaging properties such as increased penetration depth and lower tissue autofluorescence. TP-Phos was successfully used to image the endogenous ALP activity of hippocampus, kidney and liver tissues from rat.

Keywords: Alkaline phosphatase; Selectivity; Two-photon; Ortho-functionalization; Cell imaging.

1. Introduction

Alkaline phosphatase (ALP) is a family of enzymes involved in the regulation of phosphate metabolism in both prokaryotes and eukaryotes. ALP can act on a variety of biomolecules, including proteins, phosphatidates, nucleic acids and inorganic phosphates. By catalyzing the hydrolysis and transphosphorylation of monophosphate esters at alkaline pH, ALP is involved in regulating many important biological processes, including cell differentiation, bone mineralization and detoxification of bacteria endotoxin [1, 2]. Studies have also shown that abnormal levels of ALP is associated with a variety of human diseases, such as bone diseases [3, 4], liver dysfunction [5, 6], breast and prostatic cancer [7, 8], and diabetes [9, 10]. Despite these advancements in research, the diverse physiological and pathological functions of ALP still remain largely unknown. Consequently there has been growing interest in developing chemical tools for accurate and selective detection of ALP activity in living systems. Such tools will help further delineating the roles of ALP in various biological and pathological processes. Furthermore, developing chemical tools for sensing ALP might find useful applications in clinical diagnosis.

Among different methods to detect ALP activity, the fluorescent probe approach has proven to be particularly useful, especially as a nondestructive and noninvasive way to monitor the biological targets in real time. To date, a number of fluorescent probes have been reported to be able to detect ALP activity. These probes are mainly based on small-molecule fluorophores or inorganic nanomaterials [11-17]. However, the vast majority of the currently available fluorescent probes perform at short excitation wavelengths, usually in the UV-vis range. As a result, they have shallow tissue penetration depths and their application in tissue imaging is limited. In addition, most of the fluorescent probes cannot differentiate ALP from other phosphatases, such as protein tyrosine phosphatases (PTPs), resulting in poor selectivity of the probes. For example, commercially available ALP fluorescent probes such as MUP [18, 19], DiFMUP [20-22], and FDP [23-25] show similar reactivity towards ALP and other phosphatases.

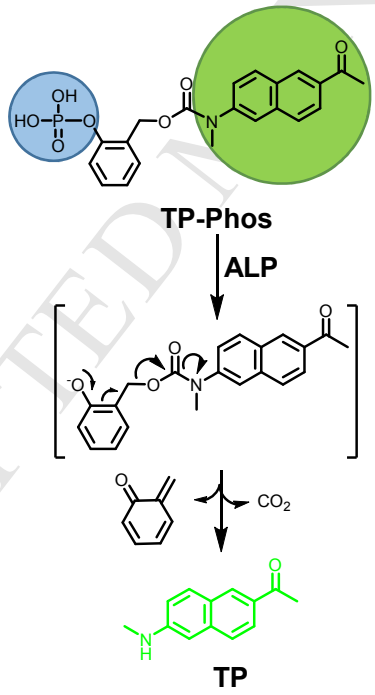

Scheme 1. Chemical structure of TP-Phos probe and its proposed "turn-on" mechanism by ALP.

To overcome the aforementioned constraints, we herein report the ALP specific fluorescent probe with two-photon properties and its imaging application in cells and tissues. The probe TP-Phos consists of three parts: a two-photon (TP) fluorophore, a phosphate recognition group, and a self-cleavable linker (Scheme 1). We hypothesize the "turn on" mechanism of the probe as follows (Scheme 1). ALP first catalyzes the

dephosphorylation of TP-Phos to produce a phenolate intermediate. Subsequently the intermediate undergoes 1,4-elimination reaction and releases ortho-quinone methide, leading to the "turn on" of fluorescence [26, 27]. Compared with the traditional one-photon fluorophore, our TP probe has a number of advantages, including increased penetration depth, low tissue auto-fluorescence and self-absorption, high resolution, reduced photo damage and photo bleaching [28, 29]. Furthermore, we specifically incorporated an ortho-functionalised phenyl phosphate group in the probe design to increase the steric hindrance between the phosphate recognition group and the active site of phosphatase. This allows ALP to be differentiated from other phosphatases. Lastly, we found that the probe showed excellent stability in DMSO and did not show any obvious decomposition after being stored at -20 ^{o}C for two years (Fig S1).

2. Material and methods

2.1. Materials and general instruments

All chemicals and solvents were purchased from commercial suppliers with the highest grade. Dulbecco's modified Eagle's medium (DMEM), fetal bovine serum (FBS), trypsin-EDTA and penicillin/streptomycin were purchased from Invitrogen. Calf intestinal alkaline phosphatase was purchased from NEB. The BIOMOL Green™ Reagent for Phosphate Detection, BML-AK111, was purchased from Enzo Life Sciences. RIPA lysis buffer and protease inhibitor cocktail were purchased from Sigma-Aldrich. 6, 8-difluoro-4-methylumbelliferyl phosphate (DiFMUP) was purchased from Sangon Biotech Co. Ltd. 4-methylumbelliferyl phosphate (4-MUP) was purchased from J&K Chemical Ltd. Other chemicals were used directly in the experiment without further purification, unless otherwise specified. Ibidi® 8-well culture plates were purchased from ibidi GmbH. C57BL/6 mice were obtained from the Laboratory Animal Services Center of the Chinese University of Hong Kong, and all experiments were performed in accordance with local guidelines. Fresh tissue slices were prepared with Leica VT1000S. ^{1}H NMR, ^{13}C NMR, and ^{31}P NMR spectra were recorded on a Bruker NMR spectrometer (400 MHz or 300 MHz). Mass spectra were obtained on a PC Sciex API 150 EX ESI-MS system using electrospray ionization (ESI). UV absorption spectra were obtained on Shimadzu 1700 UV/Vis

Spectrometer. Fluorescence signal was recorded with a FluoroMax-4 fluorescence photometer. Fluorescence images were acquired using a Leica TCS SP5 Confocal Scanning Microscope. pH value was recorded with a FiveEasy ^{TM} Fe20 pH meter.

2.2 Synthesis

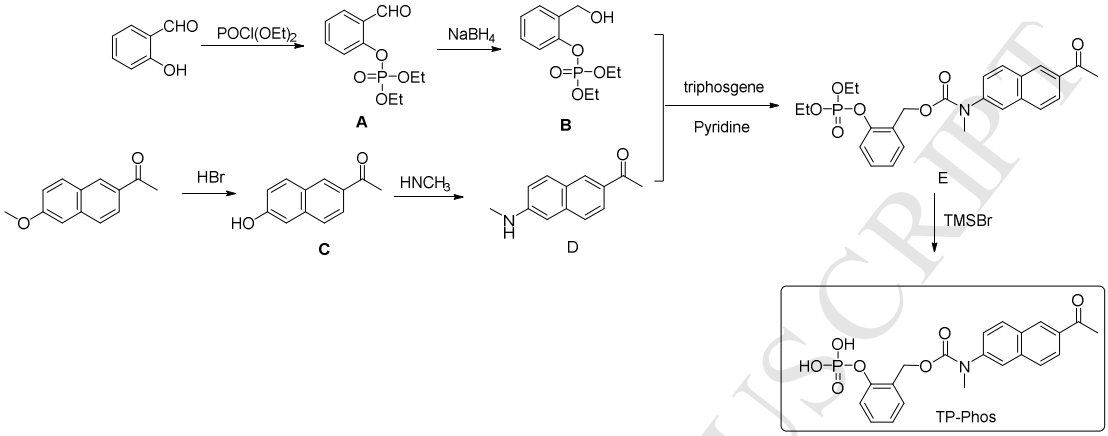

Scheme 2. Synthetic route for TP-Phos.

2.2.1 Synthesis of diethyl (2-formylphenyl) phosphate (compound A)

2-hydroxybenzaldehyde (2 mmol, 244 mg) and K_2CO_3 (10 mmol, 1.38 g) were dissolved in THF (20 mL). Diethyl phosphorochloridate (3 mmol, 432 µL) was then added to the solution and stirred at room temperature for 6 h. The organic solvent was evaporated. CH_2Cl_2 and water were subsequently added for extraction. CH_2Cl_2 phase was collected and dried with $MgSO_4$. The crude product was purified by silica gel column chromatography. Compound A was obtained with a yield of 91%. ^{1}H NMR ($CDCl_3$, 400 MHz) δ 10.42 (s, 1H), 7.90 (d, *J* = 8.0 Hz, 1H), 7.61 (t, *J* = 8.0 Hz, 1H), 7.48 (d, *J* = 8.0 Hz, 1H,), 7.31 (t, *J* = 8.0 Hz, 1H), 4.26 (t, *J* = 7.2 Hz, 4H), 1.37 (t, *J* = 7.2 Hz, 6H); ^{13}C NMR ($CDCl_3$, 100 MHz) 188.5, 152.8, 135.7, 128.8, 127.3, 125.4, 121.1, 65.1, 16.1; ^{31}P NMR ($CDCl_3$, 162 MHz) δ -6.67. ESI-MS: Calcd. for $C_{11}H_{16}O_5P$ $[M+H]^+$ 259.1; found 259.4.

2.2.2 Synthesis of diethyl (2-(hydroxymethyl)phenyl) phosphate (compound B)

Compound A (1 mmol, 258 mg) was dissolved in 20 mL of mixed solvent (E_tOH/THF/H_2O=100/20/1, v/v/v) and cooled in an ice bath. $NaBH_4$ (2 mmol, 76 mg) was added to the above solution. The reaction mixture was stirred at room temperature for 1 h. The solvent was then removed. 1 mol/L aqueous HCl was added to the residue and

extracted with ethyl acetate. Organic phase was evaporated and purified with silica gel column chromatography (ethyl acetate/Hexane, from 1/5 to 2/1). Compound B was obtained with a yield of 74%. ^{1}H NMR ($CDCl_3$, 400 MHz) δ 7.45 (d, J = 7.2 Hz,1H), 7.28 (t, J = 7.2 Hz, 1H), 7.20 (t, J = 8.0 Hz, 2H), 4.65 (s, 2H,), 4.22 (m, 4H), 1.35 (t, J = 6.9 Hz, 6H); ^{13}C NMR ($CDCl_3$, 100 MHz) 148.3, 133.1, 131.1, 129.2, 126.0, 121.0, 65.1, 60.1, 16.1; ^{31}P NMR ($CDCl_3$, 162 MHz) δ -5.06. ESI-MS: Calcd. for $C_{11}H_{18}O_5P$ $[M+H]^+$ 261.1; found 261.4.

2.2.3 Synthesis of 1-(6-hydroxynaphthalen-2-yl)ethan-1-one (compound C)

48% HBr (13.6 mL) was added to a solution containing 6-acyl-2-methoxynaphthalene (25 mmol, 5 g) in glacial acetic acid (50 mL). The mixture was stirred at 100 ^{o}C for 12 h. Excess acetic acid was then removed in vacuum. The residue was dissolved in ethyl acetate and washed with dilute $NaHCO_3$ and brine. The organic phase was dried with $MgSO_4$, and the crude product was purified with silica gel column chromatography (CH_2Cl_2/MeOH= 50/1). Compound C was obtained with a yield of 60%. ^{1}H NMR (DMSO-d_6, 300 MHz) δ 10.21 (s, 1H), 8.53 (s, 1H), 7.97 (d, J = 9.5 Hz, 1H), 7.87 (dd, J_1 = 1.7 Hz, J_2 = 8.7 Hz, 1H), 7.75 (d, J = 8.7 Hz, 1H), 7.18 (m, 2H), 2.64 (s, 3H); ^{13}C NMR (DMSO-d_6, 300 MHz) δ 197.9, 158.4, 137.6, 132.0, 131.9, 131.0, 127.1, 126.8, 124.4, 120.0, 109.3, 27.0; ESI-MS: Calcd. for $C_{12}H_{11}O_2$ $[M+H]^+$ 187.1; found 187.7.

2.2.4 Synthesis of 1-(6-(methylamino)naphthalen-2-yl)ethan-1-one (compound D)

Compound C (5 mmol, 930 mg), CH_3NH_2 (50% in H_2O) (25 mmol, 1.86 mL), $Na_2S_2O_5$ (10 mmol, 1.58 g), and H_2O (10 mL) were mixed in a 15 mL stirred autoclave and heated at 145 ℃ for 72 h. The product was collected by fi ltration and washed with water. The combined filtrate was then extracted with CH_2Cl_2. The extract was condensed in vacuo and subsequently purified by silica gel column chromatography (CH_2Cl_2/MeOH= 50/1). Compound D was obtained with a yield of 67%. ^{1}H NMR ($CDCl_3$, 400 MHz) δ 8.30 (d, J = 1.4 Hz, 1H), 7.92 (dd, J_1 = 1.8 Hz, J_2 = 8.6 Hz, 1H), 7.71 (d, J = 8.8 Hz, 1H), 7.63 (d, J = 8.6 Hz, 1H), 6.90 (dd, J_1 = 2.3 Hz, J_2 = 8.8 Hz, 1H), 6.76 (d, J = 2.3 Hz, 1H), 2.97 (s, 3H), 2.67 (s, 3H); ^{13}C NMR ($CDCl_3$, 100 MHz) δ 197.8, 149.2, 138.1, 130.8, 130.7, 130.4, 126.0, 125.9, 124.8, 118.4, 103.1, 30.4, 26.4; ESI-MS: Calcd. for $C_{13}H_{14}NO$ $[M+H]^+$ 200.1; found 200.6.

2.2.5 Synthesis of 2-((diethoxyphosphoryl)oxy)benzyl (6-acetylnaphthalen-2-yl)(methyl)carbamate (compound E)

Compound B (0.5 mmol, 130 mg) and pyridine (1.5 mmol, 121 µL) were dissolved in dry CH_2Cl_2 (10 mL) under nitrogen atmosphere. The solution was then cooled to 0 ^oC in the ice bath. Triphosgene (0.5 mmol, 148 mg) was added slowly to the solution and stirred for 6 h. Nitrogen gas was subsequently purged into the reaction mixture for 1 h to remove excess triphosgene. Compound D (84.87 mg, 0.55 mmol) was then added. The reaction solution was stirred at room temperature for 24 h. After completion of reaction, CH_2Cl_2 was added and washed with water and brine. The organic phase was dried by $MgSO_4$. The crude product was purified with silica gel column chromatography (ethyl acetate/Hexane, from 1/3 to 2/1). Compound E was obtained with a yield of 34%. ^{1}H NMR ($CDCl_3$, 300 MHz) δ 8.41 (s, 1H), 8.00 (dd, J_1 = 1.7 Hz, J_2 = 8.6 Hz, 1H), 7.91 (d, J = 8.8 Hz, 1H), 7.80 (d, J = 8.7 Hz, 1H), 7.69 (d, J = 1.9 Hz, 1H), 7.51 (dd, J_1 = 1.9 Hz, J_2 = 8.8 Hz, 1H), 7.34 (t, J = 8.5 Hz, 2H), 7.27 (td, J_1 = 1.7 Hz, J_2 = 7.6 Hz, 1H), 7.11 (t, J = 7.4 Hz, 1H), 5.29 (s, 2H), 4.13 (m, 4H), 3.43 (s, 3H), 2.68 (s, 3H), 1.26 (t, J = 7.1 Hz, 6H); ^{13}C NMR ($CDCl_3$, 75 MHz) δ 197.9, 155.2, 148.8, 143.1, 135.8, 134.5, 130.4, 130.2, 129.9, 129.8, 129.6, 128.2, 127.5, 125.5, 125.0, 124.5, 122.5, 119.7, 64.8, 62.8, 37.7, 26.7, 16.1; ^{31}P NMR ($CDCl_3$, 122 MHz) δ -4.93; ESI-MS: Calcd. for $C_{25}H_{29}NO_7P$ $[M+H]^+$ 486.2; found 486.1.

2.2.6 Synthesis of 2-(phosphonooxy)benzyl (6-acetylnaphthalen-2-yl)(methyl)carbamate (TP-Phos)

Compound E (97 mg, 0.20 mmol) was dissolved in dry CH_2Cl_2 (5 mL) at room temperature. Bromotrimethylsilane (130 µL, 1.0 mmol) was then added dropwise. The reaction mixture was stirred overnight at room temperature under nitrogen atmosphere. MeOH (3 mL) was added when the reaction completed (monitored by TLC). After the mixture was stirred at room temperature for 2 h, the solvent was removed under vacuum. The crude product was purified first with silica gel column chromatography (CH_2Cl_2/MeOH= 10/1) and then with PTLC (CH_2Cl_2/MeOH=3/1). TP-phos was obtained with a yield of 44%. ^{1}H NMR (DMSO-d_6, 300 MHz) δ 8.65 (s, 1H), 8.10 (d, J = 8.8 Hz,1H), 7.96 (m, 3H), 7.69 (dd, J_1 = 2.2 Hz, J_2 = 8.8 Hz, 1H), 7.29 (m, 3H), 7.09 (t, J = 8.0 Hz,1H),

5.21 (s, 2H), 3.41 (s, 3H), 2.69 (s, 3H); ^{13}C NMR (DMSO-d_6, 75 MHz) δ 197.8, 154.5, 143.0, 135.3, 133.9, 130.0, 129.9, 128.9, 128.6, 128.0, 127.7, 127.6, 125.6, 124.0, 123.8, 122.1, 120.3, 62.4, 37.3, 26.7; ^{31}P NMR (DMSO-d_6, 122 MHz) δ -5.91; ESI-MS: Calcd. for $C_{21}H_{21}NO_7P$ $[M+H]^+$ 430.1; found 430.4.

2.3. General procedure for fluorescence measurement

TP-Phos was dissolved in DMSO to prepare 5 mM stock solution. ALP was diluted in Tris-HCl buffer (50 mM, pH 7.4) from 10,000 U/mL stock solution, which was purchased from NEB. Appropriate amount of TP-Phos and other analytes were added to separate portions of the solution and mixed thoroughly. The reaction mixture was shaken uniformly at 37 ºC before measurement was taken. The excitation wavelength was set at 365 nm. The emission wavelength was set in the range of 400 nm to 600 nm. The slit widths of excitation and emission wavelength were both set at 5 nm.

2.4. Kinetic experiment

All kinetic measurements were performed in Tris-HCl buffer (50 mM, pH 7.4) at 37 ℃. The kinetic rate was measured by adding different concentrations of probe (0-20 μM) to the ALP solution (0.01 U/mL), and the fluorescence change was recorded every 20 seconds at 500 nm. The fluorescence calibration curve was used to calculate the rate. The parameters of the kinetic enzyme reaction, Michaelis-Menten constant (K_m), maximum rate (V_{max}) and catalytic rate constant (k_{cat}) were investigated by Lineweaver-Burk plot using software (Graphpad Prism 7.01). The results reported here are the average values of three independent experiments.

2.5. Selectivity experiment with other phosphatases

For catalytic study in vitro, the regions encoding the catalytic domains of human PTP1B (1-321), GLEEP (888-1180), MEG-2 (287-573), LYP (1-294), VHR (1-185), SSH2 (305-450), PPM1A (1-368), PPM1B (23-295) and PPM1G (1-546) were amplified by PCR and subcloned into pET-15b, pNIC-CH or pT7-7 vectors. All constructs were verified by DNA sequencing. Expression constructs were transformed into E. coli BL21 DE3 cells, and proteins were routinely purified as described in previous papers [30-32]. Protein purities were determined to be at least 90% by SDS-PAGE.

Phosphatase activities toward TP-Phos and 6, 8-difluoro-4-methylumbelliferyl

phosphate (DiFMUP) were determined by inorganic phosphate assay using the BIOMOL Green™ Reagent as described previously [33-35]. Except for metal-dependent protein phosphatases, all reactions were conducted at 25℃ in a 96-well plate in 60 µL of solution containing 50 mM Tris-HCl, pH 7.0, 1 mM EDTA, 1 mM dithiothreitol (DTT) with an ionic strength of 0.15 M adjusted with NaCl. For specific activity of PPM1A, PPM1B and PPM1G, 10 mM $MnCl_2$ was added to the reaction buffer. The reaction was stopped by adding 120 µL of BIOMOL GREEN™, and the phosphate released was determined with an end-point reading at 620 nm. The experiment was conducted under the following condition: TP-Phos (5 µM), DiFMUP (5 µM), ALP and other phosphatases (10 nM).

2.6. ALP assay in cell and tissue lysates

To prepare cell lysate, HEK 293 and HeLa cells (~1 x 10^7) were grown for 48 h in DMEM supplemented with 10 % FBS and 1% penicillin-streptomycin in 10 cm tissue culture plate. After aspirating the media, the cells were washed twice with 1 mL of cold PBS buffer. RIPA lysate buffer (500 µL) with protease inhibitor cocktail was added into the plate and incubated for 10 min on ice. Subsequently cell scraper was used to harvest the cells. The cells were transferred to a 1.5 mL tube and then passed through a 25 gauge needle 10 times to extract cell lysates. The cell lysates were incubated on ice for another 10 min and then clarified by centrifugation at 4 ℃ and 13000 x *g* for 10 min. Finally, the supernatant was transferred to a clean tube on ice for subsequent fluorescence measurement.

To prepare tissue lysate, we chose heart, liver, lung and kidney of C57BL/6 mice. 10 mg of tissue was first weighted and washed with 500 µL of cold PBS buffer twice in a Dounce homogenizer on ice. 500 µL of RIPA buffer with protease inhibitor cocktail was added and incubated for 15 min on ice. The tissue samples were then homogenized with 30-50 passes. The liquefied tissue was subsequently transferred into a 1.5 mL tube and centrifuged at 4 ℃ and 13000 x *g* for 4 min to remove any insoluble material. Finally, the supernatant was collected and transferred to a clean tube on ice for subsequent fluorescent measurement.

For ALP activity test, we used the following method. Cell lysate or tissue lysate stock solution was diluted to 0.2 mg/mL and 1 mg/ml respectively in 200 µL of Tris-HCl buffer (pH 7.4, 50 mM). TP-Phos (5 µM) was then added to the solution. After 4 min of incubation

at 37 ºC, the fluorescence intensity was measured with fluorescence photometer. The ALP activity in cell and tissue was calculated accordingly from the standard curve.

2.7. MTT test

HeLa cells were cultured in Dulbecco's modified Eagle's medium (DMEM) supplemented with 10% fetal bovine serum and appropriate amount of antibiotic (penicillin and streptomycin). Prior to the experiments, the cells were placed at 1×10^5 cells per well in a 96-well plate, followed by the addition of different concentrations of TP-Phos (0-20 μM). The cells were subsequently incubated at 37 ºC for 24 h followed by MTT assays.

2.8. Cell imaging

HeLa cells were cultured in Dulbecco's Modified Eagle's Medium (DMEM) supplemented with 10% fetal bovine serum and appropriate amount of antibiotic (penicillin and streptomycin). Approximately 1×10^5 cells were seeded in a confocal dish (20 mm) with the medium at 37 ºC. The cells were allowed to adhere to the dish under the atmosphere of 5% CO_2 and 95% air at 37 ºC and incubated for 24 h. Subsequently, the cells were incubated with TP-Phos (5 μM) in DMEM for 20 min under the atmosphere of 5% CO_2 and 95% air at 37 ºC, and then washed with DMEM. For the control experiment, the cells were pretreated with Na_3VO_4 (1 mM) for 20 min, and then incubated with TP-Phos (5 μM) for 20 min at 37 ºC and washed with DMEM. Fluorescence imaging was then carried out using Leica TCS SP5 Confocal Scanning Microscope with 40× oil and 63× water objectives under multiphoton excitation at 720 nm.

2.9. Fresh tissue imaging

Hippocampus, kidney and liver slices were all prepared from 2-week-old rat (C57 mice). The tissue slices were cut into thickness of 400 μm slices using a vibrating-blade microtome in artificial cerebrospinal fluid (ACSF: 124 mM NaCl, 3.0 mM KCl, 2.0 mM $CaCl_2$, and 1.25 mM $MgSO_4$, 26 mM $NaHCO_3$, 10 mM D-glucose, 1.25 mM KH_2PO_4). The tissue slices were incubated with TP-Phos with final concentration of 10 μM for 2 h at 37 ℃. After the slices were washed and transferred to ibidi® 8-well culture plates, imaging was performed using Leica TCS SP5 Confocal Scanning Microscope with 40× oil and 63× water objectives under multiphoton excitation at 720 nm. For inhibition experiment, Na_3VO_4 solution was first added to the slices and the mixture was incubated for 1 h.

TP-Phos was then added to the slices and the mixture was incubated for another 2 h. Subsequently, the slices were washed and imaged using a confocal microscope as previously mentioned.

3. Result and discussions

3.1. Optical properties of TP-Phos towards ALP

We first carried out absorption and emission spectra studies with the probe before and after incubation with ALP (0.01 U/mL). TP-Phos (5 μM) exhibited maximum absorption peak at 300 nm. The peak shifted to 365 nm after incubation with ALP for 20 min in Tris buffer (Fig. 1A). Fluorescence emission spectra of TP-Phos showed weak blue fluorescence with maximum emission wavelength at 450 nm when excited at 365 nm (Fig. 1B). In contrast, intense green fluorescence with maximum emission wavelength at 500 nm can be observed after incubation with 0.01 U/ml ALP for 20 min. The inserted picture in Fig. 1B, which was taken under hand UV lamp excitation before and after incubation with ALP, also proves the “turn on” of fluorescence from weak blue to bright green. We next determined two-photon absorption cross-section by investigating the two-photon excited-fluorescence spectra of TP-Phos and TP with rhodamine-6G as the reference. The product of TP-phos and ALP showed a maximal two photon cross-section of 90 GM (GM: 10^{-50} cm^4 $photon^{-1}$) at 740 nm in Tris-HCl buffer (Fig. S2). However, the two-photon absorption cross section value of TP-Phos in Tris-HCl was too small to be measured accurately. Furthermore, the reaction products of TP-Phos and ALP showed similar emission spectra under one-photon and two-photon excitations (Fig. S3).

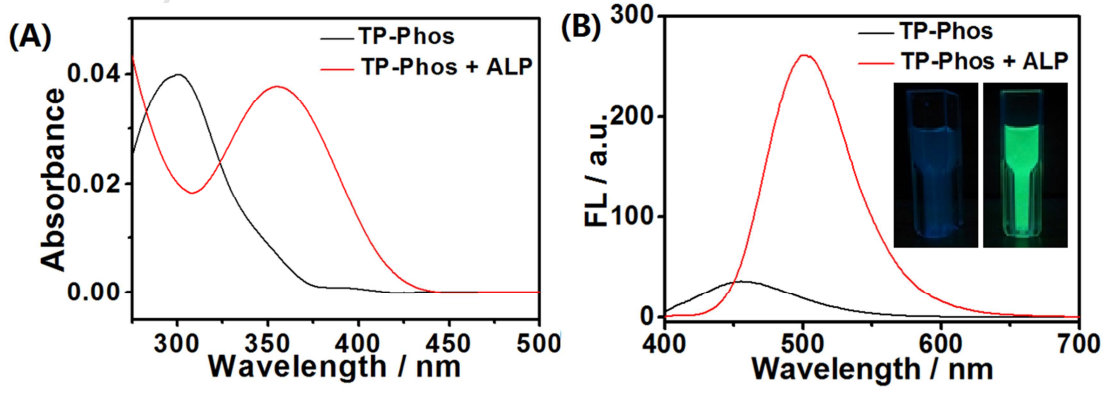

Fig. 1. Absorption (A) and fluorescent emission (B) spectra of TP-Phos(5 μM) with or without 0.01 U/mL

ALP in Tris-HCl buffer. Inset: photo of TP-Phos solution with or without ALP incubation under UV lamp excitation.

3.2. Kinetics and inhibition

Next, we moved on to study the reaction kinetics of the probe with ALP. TP-Phos (5 μM) was incubated with 0.01 U/mL ALP in Tris Buffer, and the change of the emission spectra over time was recorded. As expected, the fluorescence intensity at 500 nm increased gradually for 25 min after ALP was added. It then reached equilibrium (Fig. S4). The fluorescence intensity at 500 nm was plotted as a function of time for fixed concentration of TP-Phos (5 μM) and various concentrations of ALP (0 to 0.1 U/mL). As expected, the results show an increase in fluorescence intensity with increasing ALP concentration (Fig. 2A). The faster kinetics observed at higher concentrations of ALP signifies higher cleavage reaction rate. We further monitored the fluorescence intensity as a function of time with different concentrations of probe (0.1 to 20 μM) and fixed concentration of ALP (0.01 U/mL). The first 100 seconds of each measurement are plotted in Fig. 2B. These curves are used to determine the initial reaction rate of each hydrolysis reaction (Fig. S5). By Linewaver-Burk analysis, Km and Vmax are calculated to be 8.56 μM and 0.073 μM/s respectively. These parameters are close to the values of other ALP fluorescent probes reported in the literature [21, 22, 36]. The applicability of TP-Phos as probe to determine ALP activity was also demonstrated using a well-known inhibitor of ALP, sodium orthovanadate (Na_3VO_4) [37, 38]. ALP was mixed with different concentrations of Na_3VO_4 at 37 ^oC for 10 min. TP-Phos was then added and the mixture was incubated for another 20 min (Fig. 2C). Fluorescence was measured at various concentration points of the inhibitor. The corresponding IC_{50} was determined to be 7.39 μM, which is in good agreement with the value reported in the literature [39-41].

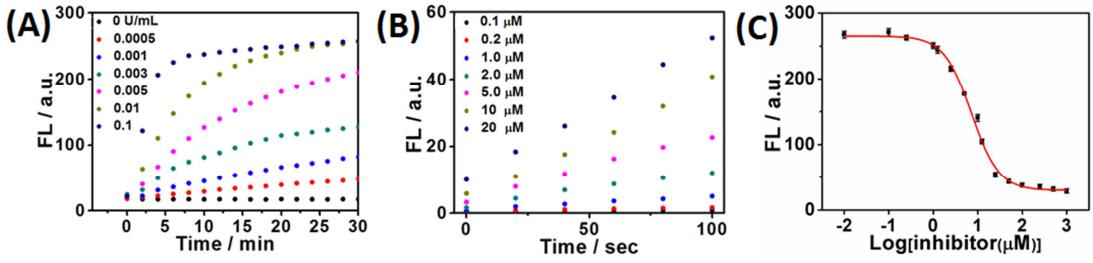

Fig. 2. (A) Time-dependent fluorescence intensity of TP-Phos (5 μM) with various concentrations of ALP (0-0.1 U/mL). (B) Time-dependent fluorescence intensity of increasing concentrations of TP-Phos (0.1-20 μM) with 0.01 U/mL ALP. (C) Inhibition study with 5 μM TP-Phos in the presence of different concentrations of Na_3VO_4. All reactions were performed in 50 mM Tris-HCl (pH 7.4) at 37 ^oC. Fluorescence intensity in 2A-2C was measured at 500 nm with excitation at 365 nm.

3.3. Detection limit of ALP

Different units of ALP (0-10 U/L) were added to TP-Phos in Tris-HCl buffer. After the reaction was incubated for 4 min, the fluorescence intensity was measured and plotted against ALP activity. The result showed a linear relationship between fluorescence intensity and ALP activity from 0.5 to 10 U/L with the fitting equation y = 9.16 [ALP] + 19.98 with R^2=0.98 (Fig. S6). The detection limit based on 3σ/slope is estimated to be 0.30 U/L.

3.4. Selective detection of ALP

The specificity of TP-Phos towards ALP versus other analytes was assessed using a series of biologically relevant species that could potentially affect the probe response in living cells, such as reactive oxygen species (ROS), reactive sulfur species (RSS), anions, and various enzymes commonly found in cells. As shown in Fig. S7, TP-Phos displayed excellent selectivity for ALP over these interferents. Furthermore, the selectivity of TP-Phos for ALP versus other phosphatases was examined in detail using classical protein tyrosine phosphatases (PTPs) (GLEPP, PTP1B, MEG-2, LYP), dual specific PTPs (VHR, SSH2) and metal-dependent Ser/Thr phosphatases (PPM1A, PPM1B, PPM1G). Fig. 3 shows the results obtained from TP-Phos in comparison with DiFMUP, a probe commonly used for ALP detection. It can be seen that after 10 min of incubation, the dephosphorylation rate of TP-Phos in the presence of ALP is more than ten folds higher than that of the other nine phosphatases tested. DiFMUP, on the other hand, shows comparable reactivity towards ALP and GLEPP, and a lower but still significant response to at least two other PTPs (PTP1B and MEG-2). Similar results were obtained after 30 min of incubation (Fig. S8). The high selectivity of our ALP probe is attributed to the ortho-functionalised phenyl phosphate group, which increases the steric hindrance of the probe to access the active site of phosphatases [42, 43]. Taken together, these results

demonstrate the excellent sensitivity and selectivity of TP-Phos towards ALP, indicating that it is a promising candidate for specific detection of ALP in live cells and tissues.

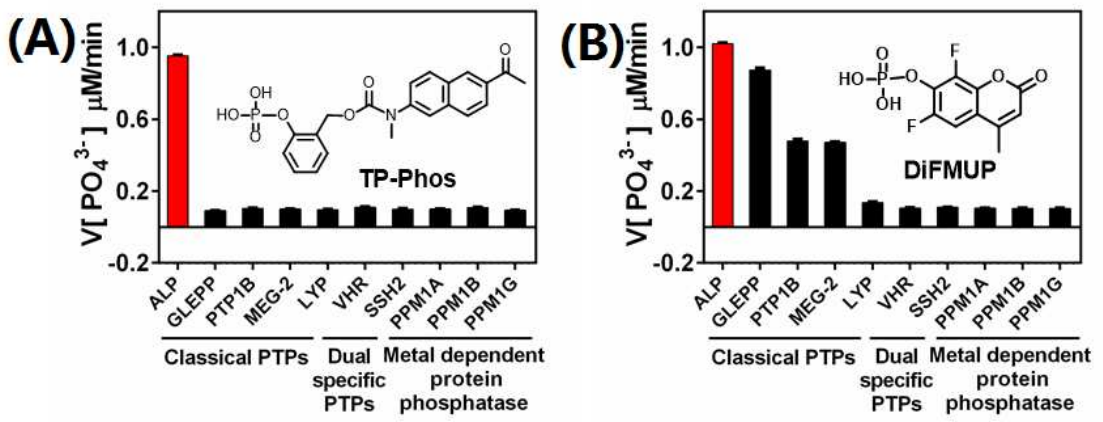

Fig. 3. Selectivity studies of TP-Phos (A) and DiFMUP (B) with ALP and various phosphatases. Incubation with phosphatases was carried out at 37 ^{o}C for 10 min. The dephosphoylation rate was calculated by measuring the amount of released phosphatase over 10 min. TP-Phos (5 μM), DiFMUP (5 μM), ALP and various phosphatases (10 nM). All reactions were performed in 50 mM Tris-HCl (pH 7.4).

3.5. ALP activity in cells and tissues lysate

To investigate the capability of TP-Phos to detect ALP activity in cells and tissues, we first prepared different cellular and tissue lysates according to the established protocol. 0.2 mg/mL cell lysate and 1 mg/mL tissue lysate were used in our study. The fluorescence intensity of TP-Phos (5 μM) was increased after the cell lysate or the tissue lysate was added. By comparing the obtained fluorescence signal with the standard curve in Fig. S6, the ALP activity was estimated to be 1.81± 0.49 U/L and 8.67±0.28 U/L in HEK 293 and HeLa cells respectively (Fig. 4A). For tissue lysate, the ALP activity was measured to be 2.51±0.21, 0.80±0.07, 4.29±0.34 and 0.99±0.12 U/L in liver, lung, kidney and heart (Fig. 4B). These results confirm the capability of TP-Phos to detect ALP activity in various cell and tissue lysates.

3.6. Two-photon imaging of ALP in cells

The potential of TP-Phos as a two-photon fluorescent probe for ALP detection was first studied in living cells. The cytotoxicity of the probe was evaluated *via* the MTT assay using HeLa cells (Fig. S9). Results show that TP-Phos at concentrations of up to 20 μM remain

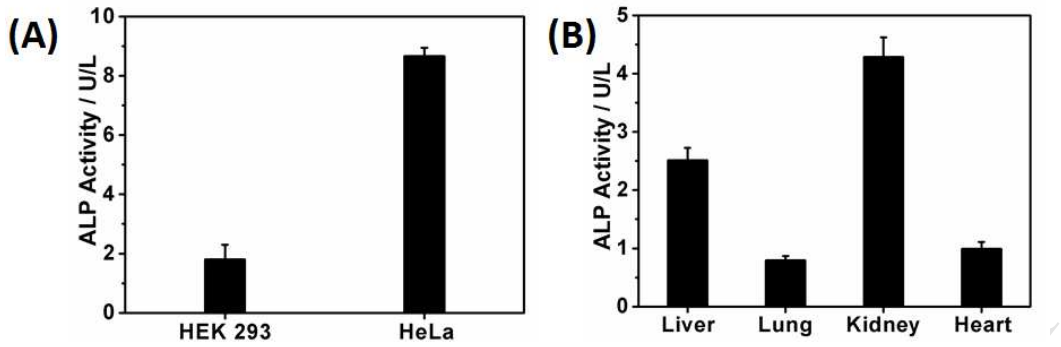

Fig. 4. (A) Measurement of ALP activity in HEK293 cell and HeLa cell lysate with 5 μM TP-Phos after 4 min of incubation at 37 ^{o}C. (B) Measurement of ALP activity in the tissue lysate of liver, lung, kidney and heart with 5 μM TP-Phos after 4 min of incubation at 37 ^{o}C.

relatively non-toxic, with cell viability remaining above 85% after 24 h of incubation. At the concentration of probe used for live cell imaging experiments (5 μM), no toxicity could be observed.

Confocal microscopy on live HeLa cells was then performed to examine whether the probe is able to detect endogenous ALP. As shown in Fig. 5A, cells incubated with TP-Phos for 20 min showed strong intracellular green fluorescence when excited at 720 nm with a two-photon confocal microscope. Interestingly, the fluorescence is mainly localized in cytoplasm. On the other hand, cells pre-incubated with 1 mM Na_3VO_4 inhibitor for 20 min prior to the addition of TP-Phos did not show any fluorescence (Fig 5A). Calculation of the pixel intensity of each image showed an approximate 8-fold reduction in fluorescence intensity in cells pre-incubated with ALP inhibitor (Fig. 5B), which is consistent with the results obtained under buffer condition. Further testing with different concentrations of Na_3VO_4 (0 μM, 250 μM, 1 mM and 2.5 mM) demonstrate that the inhibition is concentration-dependent (Fig. S11). Time-lapse fluorescence imaging of live HeLa cells upon addition of 5 μM TP-Phos shows a gradual increase in fluorescence, and the increase starts approximately 3 min after the addition of the probe (Fig. S12).

To establish more precise kinetics of probe activation in cells, the fluorescence intensities in three cytosolic regions of interest were plotted over time. The results show a linear increase of the fluorescence over time from t = 0 up to approximately 10 min. After this time frame, the probe signal appears to reach the maximum value (Fig. 5C and 5D).

Together, these results demonstrate that TP-Phos is rapidly taken up by cells (within minutes) and is able to detect ALP activity selectively and effectively in complex biological environment.

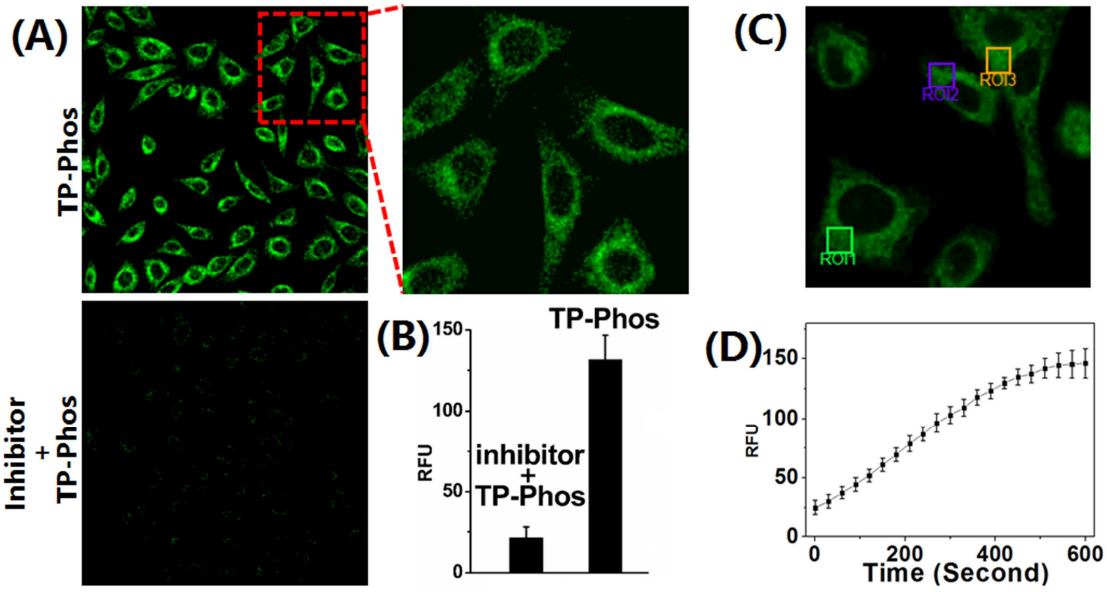

Fig. 5. (A) Confocal fluorescence images of live HeLa cells incubated with 5 μM TP-Phos for 30 min, with or without pre-incubation with 1 mM Na_3VO_4 for 20 min. (B) Fluorescence intensity of cells incubated with or without Na_3VO_4 inhibitor. (C) Three regions of interest are selected in real time fluorescence microscopy imaging experiments. Cells were treated with 5 μM TP-Phos and incubated for 10 min. (D) Real time fluorescence intensity change for the regions of interest highlighted in (C).

Encouraged by above result, we further used TP-Phos to detect ALP activity in different cell lines. We chose HEK 293 and HeLa cells as they are reported to have different ALP activity [44-45]. Both cells were put under 10 min of incubation with 5 μM TP-Phos and then washed thoroughly to remove excess probes before cell imaging. As shown in Fig. 6, HeLa cells displayed strong green fluorescence under 720 nm excitation, indicating a high expression level of ALP. In contrast, HEK 293 did not show obvious fluorescence, indicating a low level of ALP expression. Together with the result in lysates and in cell imaging, we can conclude that TP-Phos is capable of practically detecting ALP level in different cells and tissues.

The photostability of the probe was investigated with continuous irradiation at 720 nm in tissue samples. The fluorescence intensity remained almost the same after 30 min of

continuous irradiation at four randomly selected regions (Fig. S10). These results demonstrated that our probe has excellent photostability under two-photon excitation.

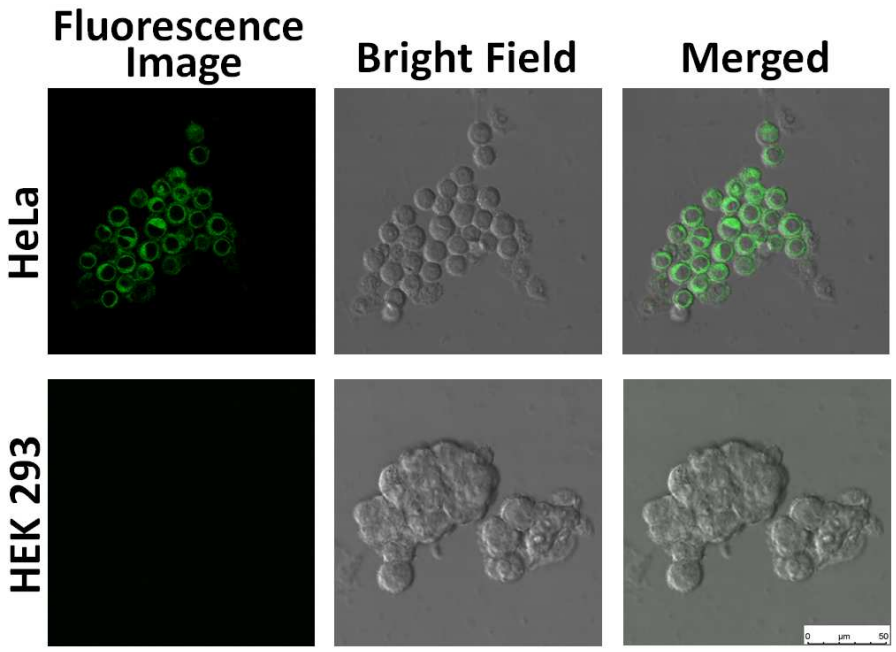

Fig. 6. Two-photon confocal images of HeLa cells and HEK 293 cells with magnification at 40 ×. Cells were allowed to adhere to the dish under the atmosphere of 5% CO_2 and 95% air at 37 ºC for 12 h. They were then incubated with TP-Phos (5 μM) for 10 min. Ex: 720 nm, Ex: 475-525 nm.

3.7. Two-photon imaging of ALP in fresh tissues

To further illustrate the advantages of our two-photon probe over previously reported ALP fluorescent probes, we performed confocal imaging experiments to study ALP activity in deep tissues. As reported in the literature, ALP is present in all the tissues throughout the entire body. In particular, it is concentrated in the liver, bones and the kidney. We performed a series of experiments to examine endogenous ALP activity using TP-Phos in different tissues, including live hippocampus, liver and kidney from rat. First, bright-field images of a hippocampus slice was used to reveal the Cornu Ammonis subfields CA1 and CA3 (Fig. 7A). At 40× magnification, two-photon fluorescence images of the slice, which was taken at a depth of 120 μm, show strong fluorescence throughout the entire sample, including CA1 and CA3. In contrast, the control tissue pre-incubated with Na_3VO_4 inhibitor

prior to the addition of probe remain almost non-fluorescent (Fig. 7C). The results confirm that the probe show selective response towards ALP.

Subsequently, imaging of liver and kidney slices at various sample depths (30-230 µm) was carried out using the *z*-scan mode of a confocal microscope. Fluorescence could be observed throughout the entire range of depths tested in the liver slice (Fig. 7B and S13), and up to a depth of 140 µM in the kidney slices (Fig. S14). Again, control samples pre-treated with Na_3VO_4 inhibitor showed the absence of fluorescence signals. These results show that TP-Phos is a suitable probe for selective imaging of endogenous ALP activity in live tissues. It provides deep tissue penetration, high selectivity and low background fluorescence.

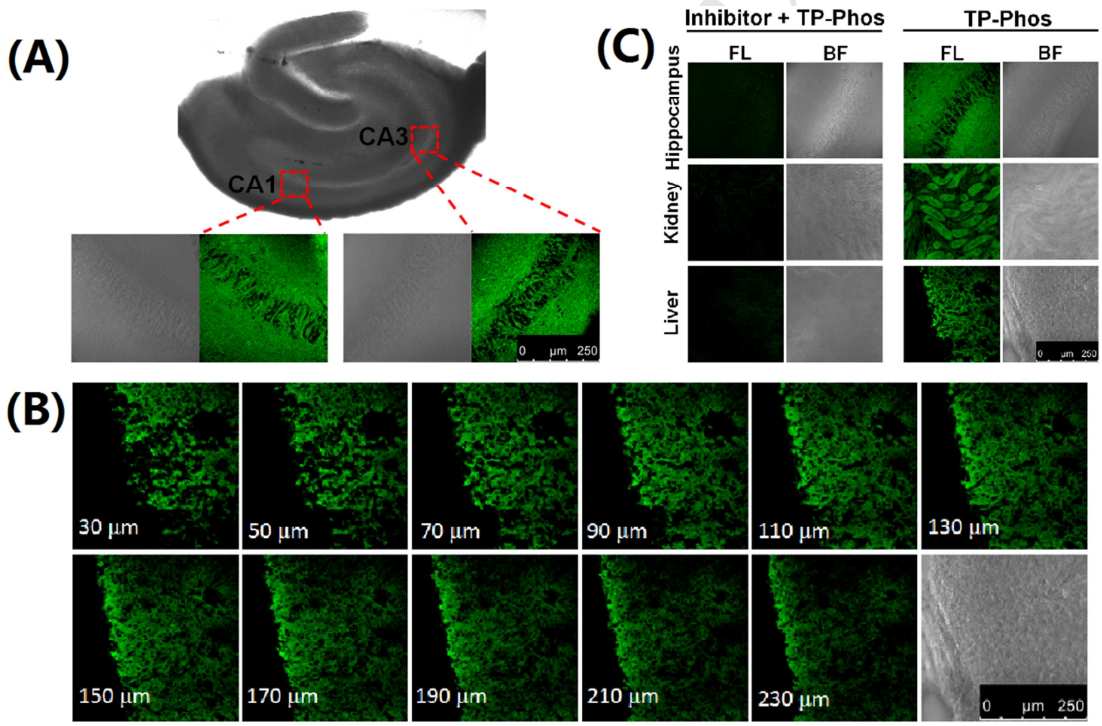

Fig. 7. (A) Two-photon images of endogenous ALP activities taken from a section of a fresh rat hippocampal slice incubated with 10 µM TP-Phos for 2 h. Images correspond to a depth of 120 µm in the tissue. Enlarged images correspond to CA1 and CA3 regions (40× magnification). (B) Two-photon images of a slice of fresh rat liver incubated with 10 µM TP-Phos for 2 h. Different images correspond to different tissue depths (from 30 to 230 µm). (C) Inhibition of ALP activity in fresh rat tissues of hippocampus, kidney and liver: pictures on the left show tissues treated with 1 mM Na_3VO_4 for 1 h prior to incubation with 10 µM TP-Phos for 2 h; picture on the right show tissues treated with TP-Phos only.

Fluorescence images were taken at excitation wavelength of 720 nm and emission band of 475 to 525 nm.

To compare the difference of resolution and penetration depth between one-photon excitation and two-photon excitation, we used different lasers as excitation sources to test the imaging with confocal fluorescence microscopy. The result clearly showed that two-photon excitation displayed better resolution and deeper penetration after 2 h of incubation of TP-Phos in rat kidney slice. For example, the imaging cannot be observed clearly under one-photon excitation when the depth is greater than 70 μm (Fig. S15), whereas the fluorescence intensity of two-photon imaging remains quite bright when the depth is around 140 μm.

4. Conclusion

In summary, we have developed a two-photon fluorescent probe, TP-Phos, for the visual detection of ALP activity in biological samples in real time. TP-Phos offer a number of advantages over previously reported probes, such as fast reaction kinetics, high sensitivity and low cytotoxicity. In contrast with MUP, DiFMUP and FDP probes, TP-Phos can differentiate between the activities of ALP from that of the other classes of phosphatases. The fact that TP-Phos relies on two-photon excitement makes it particularly attractive for tissue imaging applications. Indeed, we have shown that it is suited for detecting endogenous ALP activity in both live cells and fresh rat tissues using confocal microscopy. Nevertheless, our probe is not suitable for in vivo imaging because its green emission does not permit deep tissue penetration. We hope to address this problem by designing a two-photon probe with near-infrared emission property. We believe that the next generation probe will be useful for in vivo investigation of biological events involving ALP and it can help simplify clinical protocols for diagnosis of both liver and bone diseases.

Acknowledgements

We are grateful for the financial support from the National Natural Science Foundation of China (No. 21572190, 21471037 and 21602033), Guangdong

Natural Science Funds for Distinguished Young Scholars (15ZK0307) and the Research Grants Council of Hong Kong (No. 11302415 and 21300714).

References

[1] Coleman JE. Structure and mechanism of alkaline phosphatase. Annu. Rev. Biophys. Biomol. Struct. 1992;21:441-83.

[2] O'Brien PJ, Herschlag D. Alkaline phosphatase revisited: Hydrolysis of alkyl phosphates. Biochemistry. 2002;41:3207-25.

[3] Sharp CA, Magnusson P, Larsson L, Davie MWJ. Bone alkaline phosphatase isoforms in Paget's disease of bone. J. Bone Miner. Res. 1999;14:S540

[4] Bolarin DM. Bone-specific alkaline phosphatase protein, total alkaline phosphatase activity and lactate dehydrogenase in sera of patients with sickle cell disease. Haematologia. 2001;31:51-6.

[5] Xu Q, Lu Z, Zhang X. A novel role of alkaline phosphatase in protection from immunological liver injury in mice. Liver. 2002;22:8-14.

[6] Muraoka I, Soyama A, Takatsuki M, Tomonaga T, Hidaka M, Kanematsu T, et al. Transition of serum alkaline phosphatase isoenzymes during liver regeneration in humans. Hepatogastroenterology. 2011;58:1436-8.

[7] Ito K, Komatsu A, Kanai T, Koyama H, Hama Y, Shingu K, et al. A case of premenopausal breast cancer showing remarkable elevation of serum alkaline phosphatase level during treatment with LH-RH analog. Breast J. 2005;11:523-4.

[8] Ritzke C, Stieber P, Untch M, Nagel D, Eiermann W, Fateh-Moghadam A. Alkaline phosphatase isoenzymes in detection and follow up of breast cancer metastases. Anticancer Res. 1998;18:1243-9.

[9] Tibi L, Collier A, Patrick AW, Clarke BF, Smith AF. Plasma alkaline phosphatase isoenzymes in diabetes mellitus. Clin. Chim. Acta. 1988;177:147-55.

[10] Geszke-Moritz M, Clavier G, Lulek J, Schneider R. Copper- or manganese-doped ZnS quantum dots as fluorescent probes for detecting folic acid in aqueous media. J. Lumin. 2012;132:987-91.

[11] Song ZG, Kwok RTK, Zhao EG, He ZK, Hong YN, Lam JWY, et al. A ratiometric fluorescent probe based on ESIPT and AIE processes for alkaline phosphatase activity assay and visualization in living cells. ACS Appl. Mater. Interfaces. 2014;6:17245-54.

[12] Hou XF, Yu QX, Zeng F, Ye JH, Wu SZ. A ratiometric fluorescent probe for in vivo tracking of alkaline phosphatase level variation resulting from drug-induced organ damage. J. Mater. Chem. B. 2015;3:1042-8.

[13] Kawaguchi M, Hanaoka K, Komatsu T, Terai T, Nagano T. Development of a highly selective fluorescence probe for alkaline phosphatase. Bioorg. Med. Chem. Lett. 2011;21:5088-91.

[14] Liu SY, Pang S, Na WD, Su XG. Near-infrared fluorescence probe for the determination of alkaline phosphatase. Biosens. Bioelectron. 2014;55:249-54.

[15] Sahoo H, Hennig A, Florea M, Roth D, Enderle T, Nau WM. Single-label kinase and phosphatase assays for tyrosine phosphorylation using nanosecond time-resolved fluorescence detection. J. Am. Chem. Soc. 2007;129:15927-34.

[16] Kamiya M, Urano Y, Ebata N, Yamamoto M, Kosuge J, Nagano T. Extension of the applicable range of fluorescein: A fluorescein-based probe for western blot analysis. Angew. Chem. Int. Edit. 2005;44:5439-41.

[17] Shen CC, Li XZ, Rasooly A, Guo LY, Zhang KN, Yang MH, A single electrochemical biosensor for detecting the activity and inhibition of both protein kinase and alkaline phosphatase based on phosphate ions induced deposition of redox precipitates. Biosens. Bioelectron. 2016;85:220-25.

[18] Kobzar OL, Trush VV, Tanchuk VY, Zhilenkov AV, Troshin PA, Vovk AI. Fullerene derivatives as a new class of inhibitors of protein tyrosine phosphatases. Bioorg. Med. Chem. Lett. 2014;24:3175-9.

[19] Garcia FJ, Carroll KS. Redox-based probes as tools to monitor oxidized protein tyrosine phosphatases in living cells. Eur. J. Med. Chem. 2014;88:28-33.

[20] Sotoud H, Gribbon P, Ellinger B, Reinshagen J, Boknik P, Kattner L, et al. Development of a colorimetric and a fluorescence phosphatase-inhibitor assay suitable for drug discovery approaches. J. Biomol. Screen. 2013;18:899-909.

[21] Sanchini S, Perruccio F, Piizzi G. Rational Design, Synthesis and biological evaluation of modular fluorogenic substrates with high affinity and selectivity for PTP1B. Chembiochem. 2014;15:961-76.

[22] Jeong MS, Kim E, Kang HJ, Choi EJ, Cho AR, Chung SJ, et al. A selective Seoul-Fluor-based bioprobe, SfBP, for vaccinia H1-related phosphatase-a dual-specific protein tyrosine phosphatase. Chem. Commun. 2012;48:6553-5.

[23] Luis BS, Carpino N. Insights into the suppressor of T-cell receptor (TCR) signaling-1 (Sts-1)-mediated regulation of TCR signaling through the use of novel substrate-trapping Sts-1 phosphatase variants. FEBS J. 2014;281:696-707.

[24] Millikin R, Bianco CL, White C, Saund SS, Henriquez S, Sosa V, et al. The chemical biology of protein hydropersulfides: Studies of a possible protective function of biological hydropersulfide generation. Free Radic. Biol. Med. 2016;97:136-47.

[25] Krueger AB, Drasin DJ, Lea WA, Patrick AN, Patnaik S, Backos DS, et al. Allosteric Inhibitors of the Eya2 Phosphatase Are Selective and Inhibit Eya2-mediated Cell Migration. J. Biol. Chem. 2014;289:16349-61.

[26] Chiang Y, Kresge AJ, Zhu Y. Flash photolytic generation of ortho-quinone methide in aqueous solution and study of its chemistry in that medium. J. Am. Chem. Soc. 2001;123:8089-94.

[27] Weinert EE, Dondi R, Colloredo-Melz S, Frankenfield KN, Mitchell CH, Freccero M, et al. Substituents on quinone methides strongly modulate formation and stability of their nucleophilic adducts. J. Am. Chem. Soc. 2006;128:11940-7.

[28] Yuan L, Wang L, Agrawalla BK, Park SJ, Zhu H, Sivaraman B, et al. Development of targetable two-photon fluorescent probes to image hypochlorous Acid in mitochondria and lysosome in live cell and inflamed mouse model. J. Am. Chem. Soc. 2015;137:5930-8.

[29] Agrawalla BK, Chandran Y, Phue WH, Lee SC, Jeong YM, Wan SY, et al. Glucagon-secreting alpha cell selective two-photon fluorescent probe TP-alpha: for live pancreatic islet imaging. J. Am. Chem. Soc. 2015;137:5355-62.

[30] Xiao P, Wang X, Wang HM, Fu XL, Cui FA, Yu X, et al. The second-sphere residue T263 is important for the function and catalytic activity of PTP1B via interaction with the WPD-loop. Int. J. Biochem. Cell Biol. 2014;57:84-95.

[31] Barr AJ, Ugochukwu E, Lee WH, King ONF, Filippakopoulos P, Alfano I, et al. Large-scale structural analysis of the classical human protein tyrosine phosphatome. Cell. 2009;136:352-63.

[32] Liu J, Chen M, Li R, Yang F, Shi XR, Zhu LC, et al. Biochemical and functional studies of lymphoid-specific tyrosine phosphatase (Lyp) variants S201F and R266W. PLoS ONE. 2012;7: e43631

[33] Sun DD, Liu YN, Yu QQ, Qin XY, Yang LC, Zhou YH, et al. Inhibition of tumor growth and vasculature and fluorescence imaging using functiOnalized ruthenium-thiol protected selenium nanoparticles.

Biomaterials. 2014;35:1572-83.

[34] Cappariello A, Paone R, Maurizi A, Capulli M, Rucci N, Muraca M, et al. Biotechnological approach for systemic delivery of membrane receptor activator of NF-kappa B Ligand (RANKL) active domain into the circulation. Biomaterials. 2015;46:58-69.

[35] Lee DJ, Kessel E, Edinger D, He D, Klein PM, von Voithenberg LV, et al. Dual antitumoral potency of EG5 siRNA nanoplexes armed with cytotoxic bifunctional glutamyl-methotrexate targeting ligand. Biomaterials. 2016;77:98-110.

[36] Li L, Zhang CW, Chen GYJ, Zhu BW, Chai C, Xu QH, et al. A sensitive two-photon probe to selectively detect monoamine oxidase B activity in Parkinson's disease models. Nat. Commun. 2014;5.3276

[37] McLauchlan CC, Peters BJ, Willsky GR, Crans DC. Vanadium-phosphatase complexes: Phosphatase inhibitors favor the trigonal bipyramidal transition state geometries. Coord. Chem. Rev. 2015;301:163-99.

[38] Hulley PA, Conradie MM, Langeveldt CR, Hough FS. Glucocorticoid-induced osteoporosis in the rat is prevented by the tyrosine phosphatase inhibitor, sodium orthovanadate. Bone. 2002;31:220-9.

[39] Kim D, Moon H, Baik SH, Singha S, Jun YW, Wang T, et al. Two-photon absorbing dyes with minimal autofluorescence in tissue imaging: application to in vivo imaging of amyloid-beta plaques with a negligible background signal. J. Am. Chem. Soc. 2015;137:6781-9.

[40] Li P, Zhang W, Li KX, Liu X, Xiao HB, Zhang W, et al. Mitochondria-targeted reaction-based two-photon fluorescent probe for imaging of superoxide anion in live cells and in vivo. Anal. Chem. 2013;85:9877-81.

[41] Li JB, Wang QQ, Yuan L, Wu YX, Hu XX, Zhang XB, et al. A two-photon fluorescent probe for bio-imaging of formaldehyde in living cells and tissues. Analyst. 2016;141:3395-402.

[42] Kim TI, Kim H, Choi Y, Kim Y. A fluorescent turn-on probe for the detection of alkaline phosphatase activity in living cells. Chem. Commun. 2011;47:9825-7.

[43] Kim TI, Jeong MS, Chung SJ, Kim Y. An iminocoumarin-based fluorescent probe for the selective detection of dual-specific protein tyrosine phosphatases. Chem-Eur J. 2010;16:5297-300.

[44] Tan Y, Zhang L, Man KH, Peltier Raoul, Chen G, Zhang H, et al. Reaction-based off−on near-infrared fluorescent probe for imaging alkaline phosphatase activity in living cells and mice. ACS Appl. Mater. Interfaces. 2017;9:6796–803.

[45] Schmid F, Fliegert R, Westphal T, Bauche A, Guse AH. Nicotinic acid adenine dinucleotide phosphate (NAADP) degradation by alkaline phosphatase. J. Biol. Chem. 2012;287:32525−34.